npj | natural hazards

Article

https://doi.org/10.1038/s44304-025-00124-0

Substantial increase in wildfire danger conditions under anthropogenic climate change in Southwest France

Check for updates

Marine Lanet[1] ✉, Laurent Li[1] & Hervé Le Treut[2]

Wildfires are an increasing concern under climate change, which may raise the frequency and intensity of fire-prone conditions. Here we assess summer wildfire danger evolution in Southwestern France under three climate scenarios (Representative Concentration Pathways RCP2.6, RCP4.5 and RCP8.5), using six climate models. Alongside the Fire Weather Index (FWI), widely used by operational services to assess daily fire danger, a complementary index, SM6-T3-VPD3 (soil moisture integrated backward to 6 months, surface air temperature and vapour pressure deficit backward to 3 months), is also used to assess prolonged hot and dry conditions. Results indicate that under the highest emission scenario, the probability of extreme compound hot and dry events increases from 0.04 to 0.49 in August during the twenty-first century. Even under the lowest emission scenario, their likelihood increases from 0.03 to 0.15. Therefore, this study underscores the importance and complementarity of mitigation and adaptation strategies in addressing wildfire danger.

The expression of extreme wildfire generally follows the definition of Tedim et al. that considers both the underlying processes and their outcomes. This definition is based on fire spread and behaviour parameters, as well as the difficulty of suppression[1]. In the last decades, extreme wildfires had severe environmental and socio-economic impacts. In Canada in 2023, 18.5 million ha were burnt, which required the evacuation of 234,000 people. The severity of this wildfire season has been associated with a combination of interrelated climatic drivers, including early snowmelt, prolonged drought in western Canada, and a rapid shift toward drought conditions in the east. These factors coincided with exceptional surface warming—particularly during May and June—when average daily maximum temperatures rose by 8.11 °C. This warming pattern corresponded with persistent elevated geopotential height anomalies, which further intensified surface temperatures through enhanced subsidence[2,3]. In 2015, 2017 and 2018, fire suppression costs reached more than 1.4 billion dollars each year[4]. In 2009, Black Saturday bushfires in the Australian state of Victoria resulted in the loss of 173 lives and the destruction of over 2000 homes[5]. The event was driven by extreme fire weather conditions, characterised by daytime temperatures exceeding 45 °C, strong surface winds, and exceptionally dry atmospheric conditions—marking some of the most severe fire weather ever recorded in the region[6,7]. Ten years later, the Black Summer fires of 2019–2020 in Australia burnt 5.8 to 8.1 million ha, which emitted up to 830 million tonnes of CO2eq. It is estimated that 3 billion animals were lost or displaced, with possible extinctions, and that national financial impacts are over 8 billion dollars[8–10]. The season was marked by record-breaking fire weather conditions, as indicated by the Australian Forest Fire Danger Index (FFDI), alongside atmospheric instabilities that generated strong and highly variable wind patterns[11–13]. In 2024, the United States allocated approximately $4.79 billion to wildfire suppression efforts, a significant increase compared to the $200 million spent in 1994[14].

In Europe, the exceptional 2017 wildfire season in Portugal caused 114 fatalities[15]. The June fires were associated with a record-breaking heatwave linked to a subtropical ridge, producing extremely high temperatures, low humidity, and atmospheric instability conducive to convective activity. In October, persistent southerly dry winds, combined with prolonged drought and elevated temperatures, created conditions that favoured rapid fire spread[16]. The next year, in 2018, burnt area in Sweden reached 835% of the 2008-2017 average, 827% in Latvia and 706% in Germany, showing that not only Mediterranean countries are exposed to wildfire danger[17]. It is also the year when the Mati wildfire in the Attica region in Greece had dramatic impacts as it resulted in 102 deaths and burnt 1400 ha of land, 1200 buildings, and 300 vehicles[18]. Although not among the largest fires in the region—let alone globally—it ranks as one of the deadliest worldwide in terms of human fatalities[17]. It was favoured by very high winds (90–120 km/h) and air temperature above 40 °C. In 2021, Greece experienced a very active wildfire season that caused a significant increase in air pollution[19]. In 2022, by the end of September, the fire season in southwestern Europe (Portugal, Spain, and France) had resulted in a burnt area nearly three times

[1]LMD/IPSL, Sorbonne Université, ENS, Université PSL, École Polytechnique, Institut Polytechnique de Paris, CNRS, Paris, France. [2]Institut Pierre-Simon Laplace, Sorbonne Université, Paris, France. ✉e-mail: marine.lanet@lmd.ipsl.fr

greater than the annual average recorded between 2006 and 2021. In Southwestern France in particular, 33,052 ha were burnt, representing 16 times the 2006–2021 average[20], and leading to important ecological and socio-economic damages[21]. In 2023, Greece experienced the largest single wildfire recorded in the European Union (EU) since 2000, with a burnt area of 96,000 ha. In total, the 2023 wildfire season in Greece resulted in a burnt area of 175,759 ha, the highest record since 2007, causing 24 deaths[22].

The question of the role of climate change in the occurrence of extreme wildfire events has been raised. Attribution studies have revealed that climate change often increased the likelihood of weather conditions prone to extreme wildfires[21,23–29]. While numerous studies have examined historical records and identified increasing trends in fire weather days[30–32], recent research has also focused on projecting the climatic drivers of wildfire activity[33,34]. Wildfires' ignition and spread are not only influenced by climate conditions, but also by the state of vegetation, topography, and anthropogenic factors, such as land management, land conversion, population density and the wildland-urban interface (WUI)[35–40]. In this article, we focus on climate conditions, as they play a crucial role in modulating wildfire activity worldwide, especially in the context of climate change[41–45]. We employ the terminology presented by Chuvieco et al. that defines the wildfire risk as the combination of danger, exposure and vulnerability[46]. Here, we mainly focus on the wildfire danger.

The most widely used index to assess weather conditions prone to wildfires is the Canadian Forest Fire Weather Index (FWI)[47]. It informs on the daily variability of the wildfire danger, also accounting for monthly dryness. It consists of five key components: the Fine Fuel Moisture Code (FFMC), Duff Moisture Code (DMC), Drought Code (DC), Build-Up Index (BUI), and Initial Spread Index (ISI). The FFMC, DMC, and DC are meteorological indices that provide moisture assessments at various litter depths (1.2, 7 and 18 cm, respectively). The deeper the soil layer, the longer the timescale over which it responds to moisture changes. The BUI is derived from the DMC and DC. It represents long-term drying of bulkier fuels, assuming a sufficient availability of dead fuel, and is linked to the potential intensity of fires. In contrast, the ISI reflects the combined effects of fine fuel moisture and wind speed, which influence the rate at which fires can spread. Ultimately, the FWI is determined using both the BUI and ISI, offering an estimate of fire danger and intensity under prevailing weather conditions, should ignition occur. The FWI is strictly a meteorological index that estimates fire danger based on these components, without directly accounting for actual fuel loads or conditions[48,49]. The index is unsuitable for averaging and should be used as its single daily value only. Nevertheless, it can be transformed into the Daily Severity Rating (DSR) and subsequently averaged over time to produce the Seasonal Severity Rating (SSR) (see "Methods")[47].

The FWI analysis is usually based either on fixed threshold intensities (e.g. FWI = 15, 30, or 45, corresponding to moderate, high or very high danger)[50–54], or on percentiles (e.g. 90th or 95th percentiles)[55,56]. FWI thresholds associated with specific danger might be region-dependent[57]. The graduated alert thresholds, indexed to the FWI and corresponding to the phased deployment of firefighting resources, vary from one region to another to account for the specific characteristics of each territory, as recommended[49]. In this regard, using percentiles on a reference period appears to be a relevant metric to analyse high danger for a given location. Other indices were also used to assess the increase in wildfire potential and magnitude, such as the Keetch–Byram Drought Index (KBDI)[58–60], or the McArthur Forest Fire Danger Index (FFDI)[61,62]. These indices are usually updated daily to monitor the wildfire danger evolution and adapt operational decisions[63–65]. Developed in the USA, the KBDI assesses the cumulative soil moisture deficit in the upper soil layers based on air temperature and rainfall[66]. The FFDI not only assesses drought conditions, but as the FWI, it also aims at evaluating fire behaviour and suppression difficulty, integrating two other variables: wind speed and relative humidity[67,68].

Two primary factors control the extent of burnt area: extremely hot, dry and windy days, referred to as "weather anomalies", typically measured by the FWI or similar indices such as the FFDI, and relatively long dry periods, defined as "climate anomalies" at the monthly or seasonal scale[69]. Summer 2022 in Southwest France is a good example of such long-term "climate anomaly". Climate conditions were exceptional as they featured a combination of a long-term drought that started in late winter, and three successive heatwaves[21,70], leading to the most devastating wildfires in the region since 1949. Previous studies underlined the influence of long-term soil dryness, temperature and vapour pressure deficit (VPD) on the wildfire danger[71–75]. Lanet et al.[21] created a seasonal compound index that correlates with large burnt areas during July and August in Southwestern France. It combines standardised soil moisture integrated over 6 months with standardised temperature and VPD integrated over three months to analyse compound dry and hot events on a seasonal timescale. These events are associated with prolonged vegetation moisture stress and complement the FWI in specifically analysing the long-term drivers of extensive burnt areas in Southwestern France. Aggregating wind speed over multi-month periods would obscure the physical interpretation of the weather–fire relationship by blending distinct synoptic regimes. In Southwestern France, a coastal region, westerly winds typically transport moist air masses from the Atlantic, while easterly flows are generally associated with drier conditions[76]. To preserve this meteorological specificity, wind speed is not accounted for in the seasonal compound index. However, at daily timescales, wind speed remains a critical variable in modulating fire behaviour in certain regions and seasons[76]. Its influence is notably captured through the Initial Spread Index (ISI), a key component of the FWI[77]. Atmospheric instability, which can influence fire behaviour by promoting pyroconvection[78], is not included in this seasonal compound index neither, as its effects are more relevant at daily timescales. This factor is likewise excluded from the formulation of the FWI.

This study aims to assess how two key determinants influencing the extent of summer burnt areas—long-term climate anomalies and short-term weather anomalies, as identified by Pereira et al.[69]—will evolve in response to climate change in Southwestern France. Previous research conducted in Southwestern France during the summer months has shown that the FWI and its short-term component, the ISI, are correlated with large wildfires. In contrast, its longer-term indicators—such as the DC, DMC, and BUI—do not exhibit such correlations and appear less effective in capturing prolonged fire-conducive conditions[21]. Further analysis supports this finding, with a strong linear relationship observed between ISI and FWI, evidenced by a Pearson correlation coefficient of 0.94 (see Fig. S1 in the Supplementary Material). Additionally, Kendall correlation coefficients, which account for non-linear relationships, indicate that the FWI is primarily correlated with its short-term components (see Fig. S2). Therefore, the current study combines an evaluation on a daily timescale using the FWI provided by the Copernicus Climate Change Service (C3S), with an evaluation on the seasonal timescale using an index characterising specifically long-term compound dry and hot conditions, computed using CMIP6 climate data. Adapted from the index developed by Lanet et al.[21] (see "Methods"), this second index, SM6-T3-VPD3, combines surface soil moisture integrated over 6 months (SM6), and surface air temperature and VPD over 3 months (T3 and VPD3, respectively). Several studies have highlighted the role of these three variables in increasing wildfire danger. High VPD and temperature induce vegetation drying, therefore increasing the wildfire danger[32,75,79–83]. Prolonged soil moisture deficits can also lead to desiccation of both live and dead fuels, thus creating conditions favourable for large and intense fires[71,73]. Soil moisture varies over longer timescales than temperature and VPD, which justifies the use of a longer integration period for this variable[21] (see "Methods" for more details on the index development).

Fire-prone extreme weather conditions are defined on a reference period (1991–2020). The evolution of the likelihood of such event over the twenty-first century is analysed (see "Methods"). We report an application of the methodology to Southwestern France (longitude between −1.25° and 1.25°, and latitude between 43.73° N and 45° N), a region that experiences wildfires on an annual basis. The study area includes the Landes Forest, an intensively managed and predominantly homogeneous landscape of

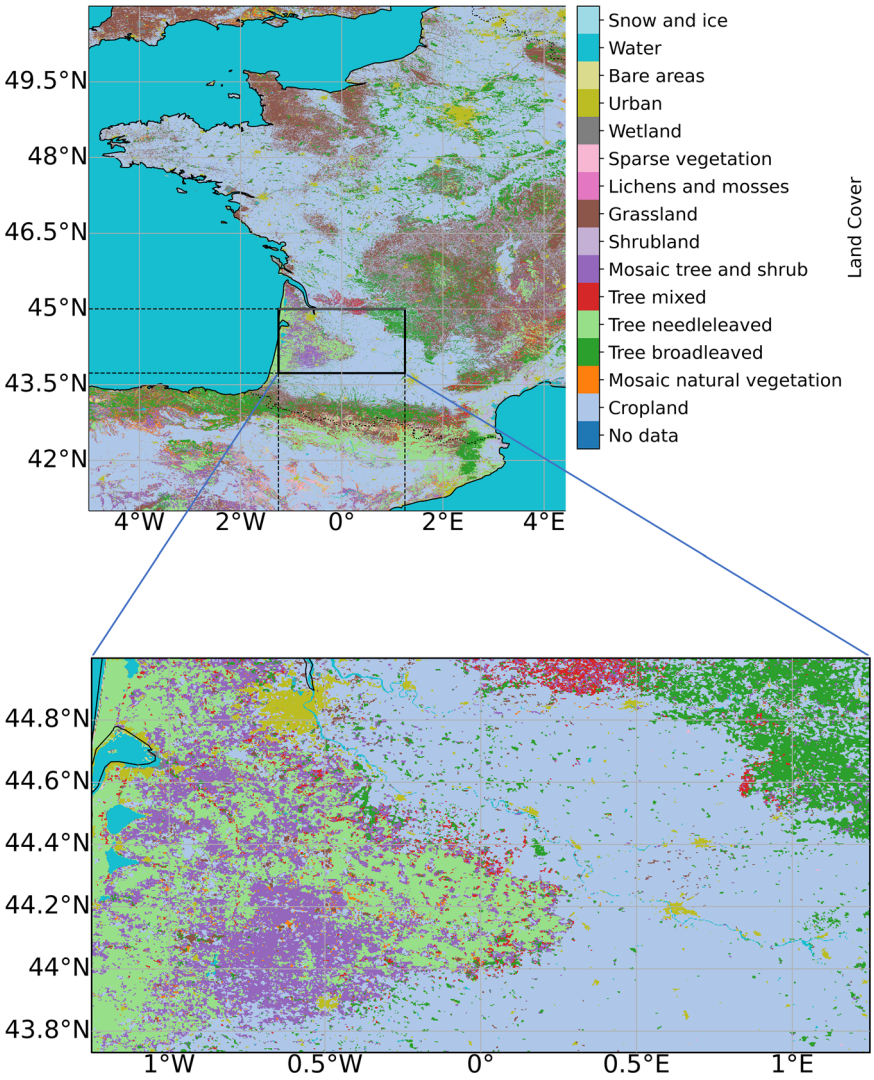

Fig. 1 | Location and land cover of the study area (2022 land cover data from ESA Climate Change Initiative).

maritime pine (*Pinus pinaster*) (see Fig. 1), which is of central importance to the regional timber industry. Wildfires in the region can be triggered by natural phenomena, accidental human activity, or criminal arson[84]. We focus on July and August, as they are the hottest and driest months in the studied region. This period also coincides with the peak of tourist activity, which further increases the risk of ignition due to heightened human presence in forested areas—often by individuals less familiar with fire prevention practices than local residents[85]—and exacerbates emergency response challenges. Although the wildfire season typically extends from May to October, the months of July and August alone account for 78.6% of the total burnt area between 2006 and 2024, according to the BDIFF (*Base de Données des Incendies de Forêt en France*) database[84] (see Fig. 2).

Results

Daily danger projection

The analysis of the FWI projections provided by the C3S (see "Methods" for the evaluation and selection of the models) reveals that daily fire-weather extremes, as defined by the 90th and 75th percentiles on 1991–2020 (FWI_{90} and FWI_{75}, respectively), will become more frequent, especially in August (see Fig. 3). Under the RCP4.5 climate scenario, events that were considered rare during the reference period with only an 11% chance of happening (FWI_{90}) are expected to become more common, with their likelihood increasing to 23% at the end of the century. For the month of July, this means an increase from 10% to 16%. Meanwhile, FWI_{75} events will see their probability increases from 0.27 to 0.44 (from 0.23 to 0.35 in July).

The emission scenario followed over the next few years will have a strong influence on the evolution of extreme fire weather (see Fig. 4). The highest emission scenario, RCP8.5, projects a strong increase in the frequency of extreme conditions propitious to wildfires as the survival probability of the 90th percentile increases from 0.11 to 0.29 in August (from 0.09 to 0.33 in July). Conversely, under the lowest emission scenario, RCP2.6, the frequency of extreme fire-weather might slightly decrease from 0.12 to 0.08 in August (from 0.13 to 0.11 in July) by the end of the century. The decreasing trend observed under the RCP2.6 scenario may be attributed to a combination of decreasing wind speed (Fig. S3), increasing precipitation (Fig. S4), and rising relative humidity (Fig. S5). The mid-century dip observed in the RCP4.5 scenario appears to result from a slight decline in temperature (Fig. S6) and wind speed, accompanied by increases in both precipitation and relative humidity. In contrast, the increasing trend projected under the RCP8.5 scenario is likely driven by a pronounced rise in temperature and wind speed, coupled with a substantial decrease in precipitation and relative humidity.

Seasonal danger projection based on marginal probability

We use CMIP6 simulations to analyse SM6-T3-VPD3 projections (see "Methods" for the evaluation and selection of the models). A reference compound hot and dry event on 1991–2020 can be defined either by setting the marginal probabilities of the three variables studied, or by setting the joint probability of these three variables.

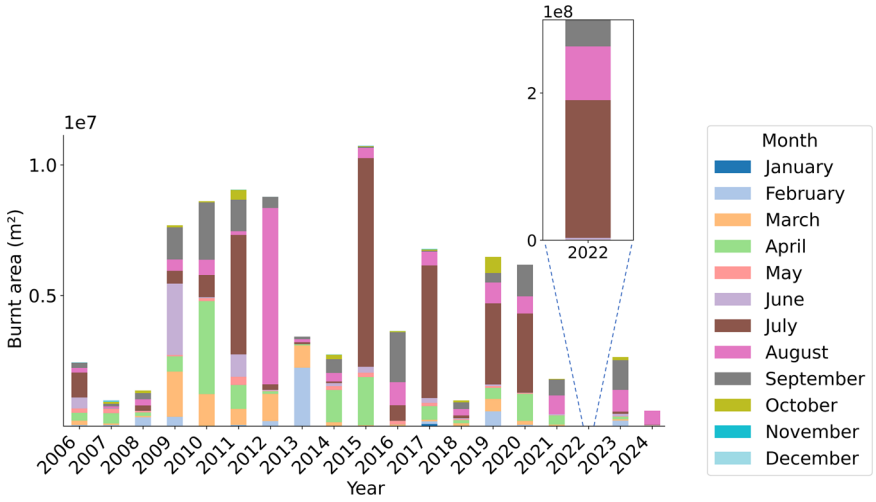

Fig. 2 | Burnt area in Southwestern France from 2006 to 2024 (BDIFF data).

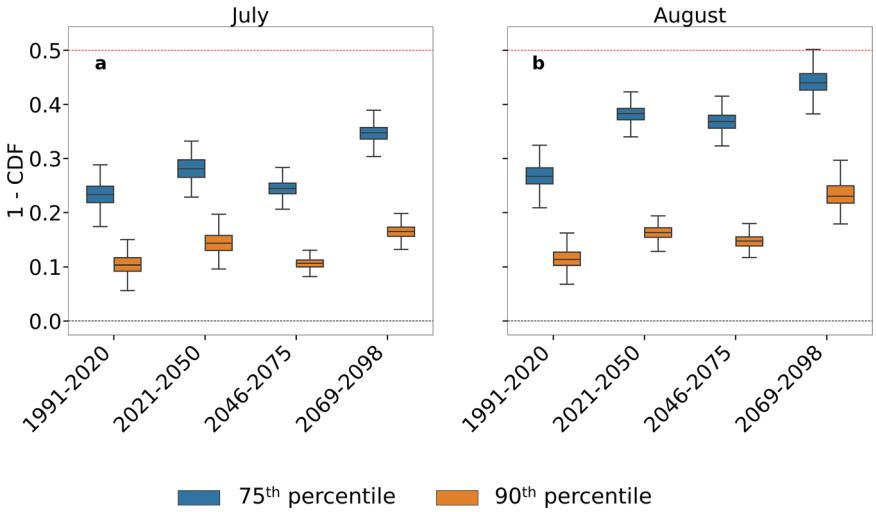

Fig. 3 | Increase in FWI_{75} and FWI_{90} events during the twenty-first century. Evolution of the survival probability, defined as 1 − Cumulative probability (1 − CDF), of the 75th (blue) and 90th (orange) percentiles of the FWI (defined on the reference period 1991–2020) in July (**a**) and August (**b**) under RCP4.5 scenario. A box spans from the first quartile to the third quartile, with a line inside the box indicating the median (second quartile). The whiskers extend to points that lie within 1.5 interquartile range of the lower and upper quartile. The horizontal red dashed line represents a probability of 0.5.

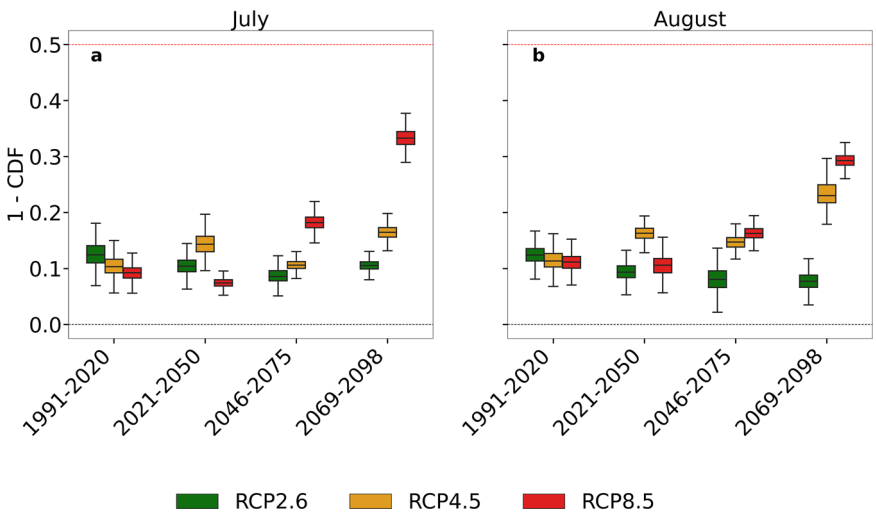

Fig. 4 | Increase in FWI_{90} events during the twenty-first century under three RCPs. Evolution of the survival probability (1-CDF) of the 90th percentile of the FWI (defined on the reference period 1991–2020) in July (**a**) and August (**b**) under RCP2.6 (green), RCP4.5 (orange) and RCP8.5 (red) scenarios. A box spans from the first quartile to the third quartile, with a line inside the box indicating the median (second quartile). The whiskers extend to points that lie within 1.5 interquartile range of the lower and upper quartile. The horizontal red dashed line represents a probability of 0.5.

First, we define a reference compound hot and dry event on 1991–2020 as a combination of the 10th percentile of SM6, and the 90th percentile of both T3 and VPD3. To evaluate the impact of the percentiles used on the results, another more moderate compound dry and hot event is analysed, defined by the 25th percentile of SM6, and the 75th percentile of both T3 and VPD3. These two reference events are called $SM6_{10}$-$T3_{90}$-$VPD3_{90}$ and $SM6_{25}$-$T3_{75}$-$VPD3_{75}$, respectively.

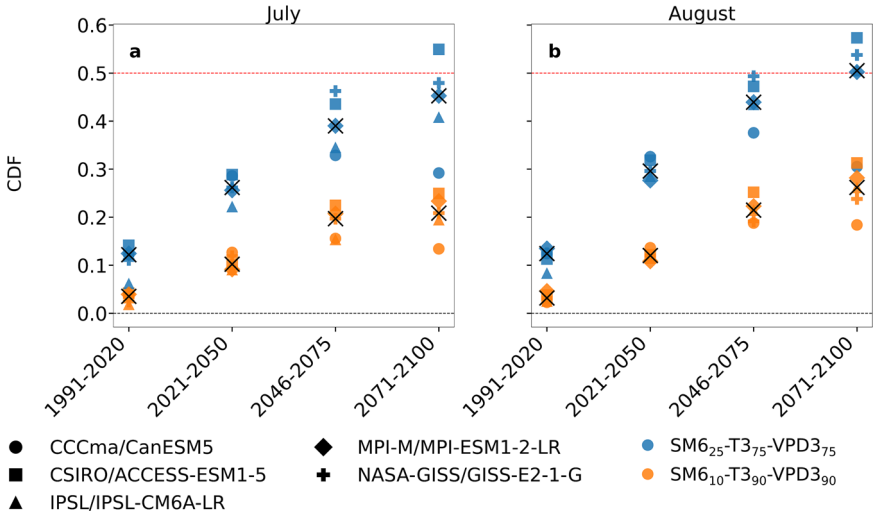

Fig. 5 | Increase in hot and dry conditions frequency during the twenty-first century. Evolution of the cumulative probability (CDF) of SM6$_{25}$-T3$_{75}$-VPD3$_{75}$ (blue) and SM6$_{10}$-T3$_{90}$-VPD3$_{90}$ (orange) in July (**a**) and August (**b**) under SSP2-4.5 scenario. The crosses represent the medians of the five models and the dots each individual model. The horizontal red dashed line represents a cumulative probability of 0.5.

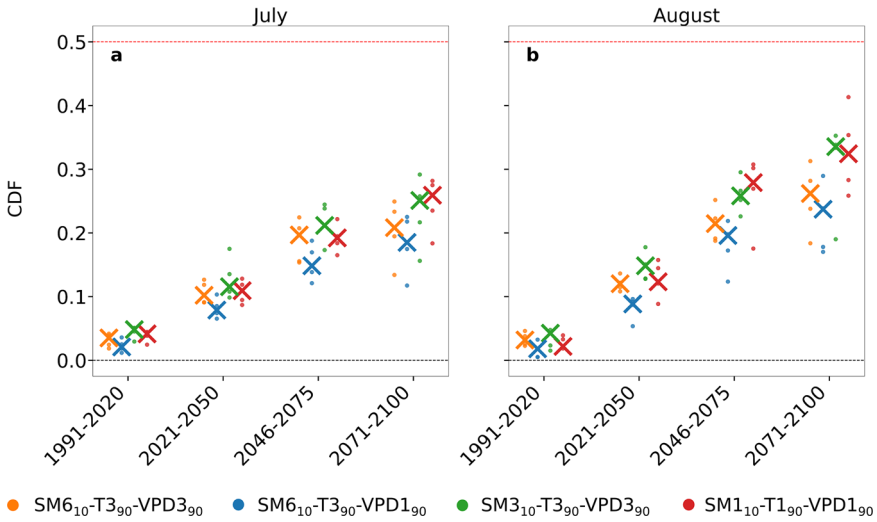

Fig. 6 | Increase in extreme hot and dry conditions characterised by four seasonal compound indices. Evolution of the cumulative probability (CDF) of SM6$_{10}$-T3$_{90}$-VPD3$_{90}$ (orange), SM6$_{10}$-T3$_{90}$-VPD1$_{90}$ (blue), SM3$_{10}$-T3$_{90}$-VPD3$_{90}$ (green), and SM1$_{10}$-T1$_{90}$-VPD1$_{90}$ (red) in July (**a**) and August (**b**) under SSP2-4.5 scenario. The crosses represent the medians of the five models and the dots the five models. The horizontal red dashed line represents a cumulative probability of 0.5.

Similarly to the FWI study, the analysis of the seasonal compound index shows that fire weather will increase in the twenty-first century. Under the SSP2-4.5 climate scenario, a compound dry and hot event characterised by SM6$_{10}$-T3$_{90}$-VPD3$_{90}$ has a joint probability increasing from 0.03 for 1991–2020 to 0.26 for 2071–2100 in August (from 0.04 to 0.21 in July), considering the median across the five models. This means that 26% of the August months will be hotter and dryer than this reference extreme event at the end of the century, while they were only 3% in 1991–2020. Under the SSP2-4.5 climate scenario, a slightly less dry and hot July month characterised by SM6$_{25}$-T3$_{75}$-VPD3$_{75}$ has a joint probability increasing from 0.12 for 1991–2020 to 0.45 for 2071–2100. In August, the increase in frequency of extreme events is even more pronounced, with a probability of SM6$_{25}$-T3$_{75}$-VPD3$_{75}$ rising from 0.12 for 1991–2020 to 0.51 for 2071–2100 (see Fig. 5). This means that a rare event in the reference period will become normal conditions at the end of the century.

To evaluate the influence of the definition of the climate index used to perform this seasonal analysis, three other combinations of variables are analysed by varying the integration time: SM6-T3-VPD1, SM3-T3-VPD3, SM1-T1-VPD1 (see "Methods" for further details on the selection of these indices). The strongest increase in August compared to July in the frequency of occurrence of an extreme event is also noticeable with the other compound indices (SM6$_{10}$-T3$_{90}$-VPD1$_{90}$, SM3$_{10}$-T3$_{90}$-VPD3$_{90}$, SM1$_{10}$-T1$_{90}$-VPD1$_{90}$). Whatever the seasonal compound index used, the probabilities of extreme dry and hot conditions are close in the first half of the century. Probabilities slightly differ across indices at the end of the century (see Fig. 6). In August, the probability of SM3$_{10}$-T3$_{90}$-VPD3$_{90}$ reaches 0.34 in 2071–2100, while the probability of SM6$_{10}$-T3$_{90}$-VPD1$_{90}$ reaches 0.24. In July, when using SM1$_{10}$-T1$_{90}$-VPD1$_{90}$ to characterise the extreme event the joint probability increases from 0.04 for 1991–2020 to 0.26 for 2071–2100, using SM3$_{10}$-T3$_{90}$-VPD3$_{90}$ from 0.05 to 0.25, and using SM6$_{10}$-T3$_{90}$-VPD1$_{90}$ from 0.02 to 0.19. The slightly strongest increase in probability for SM1$_{10}$-T1$_{90}$-VPD1$_{90}$ and SM3$_{10}$-T3$_{90}$-VPD3$_{90}$ compared to the two other indices might be due to the fact that the increase in temperature and the drying trends are more pronounced in summer[86]. As SM6-T3-VPD1 and SM6-T3-VPD3 integrate climate variables from spring and late winter, the increase might be slightly less pronounced.

Similarly to the FWI study, the analysis of the three SSPs reveals a strong influence of the scenario followed on the evolution of the frequency of compound dry and hot conditions (see Fig. 7). Considering the lowest emission scenario, SSP1-2.6, the joint probability of a compound extreme event characterised by SM6$_{10}$-T3$_{90}$-VPD3$_{90}$ increases from 0.03 to 0.15 in August (from 0.04 to 0.09 in July). Considering the highest emission scenario, SSP5-8.5, extreme events become normal conditions as their probability increases from 0.04 to 0.49 in August (from 0.04 to 0.38 in July). This suggests that by the end of the century (2071–2100), there will be a 49% probability (about 1 in 2) that an August month will be hotter and drier than

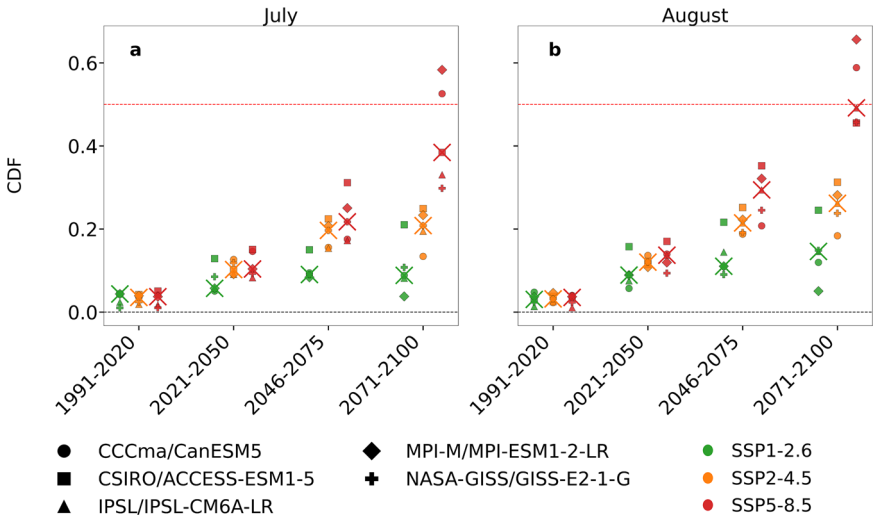

Fig. 7 | Increase in extreme hot and dry conditions under three scenarios. Evolution of the cumulative probability (CDF) of $SM6_{10}$-$T3_{90}$-$VPD3_{90}$ in July (**a**) and August (**b**) under SSP1-2.6 (green), SSP2-4.5 (orange) and SSP5-8.5 (red) scenarios. The crosses represent the medians of the five models and the dots each individual model. The horizontal red dashed line represents a cumulative probability of 0.5.

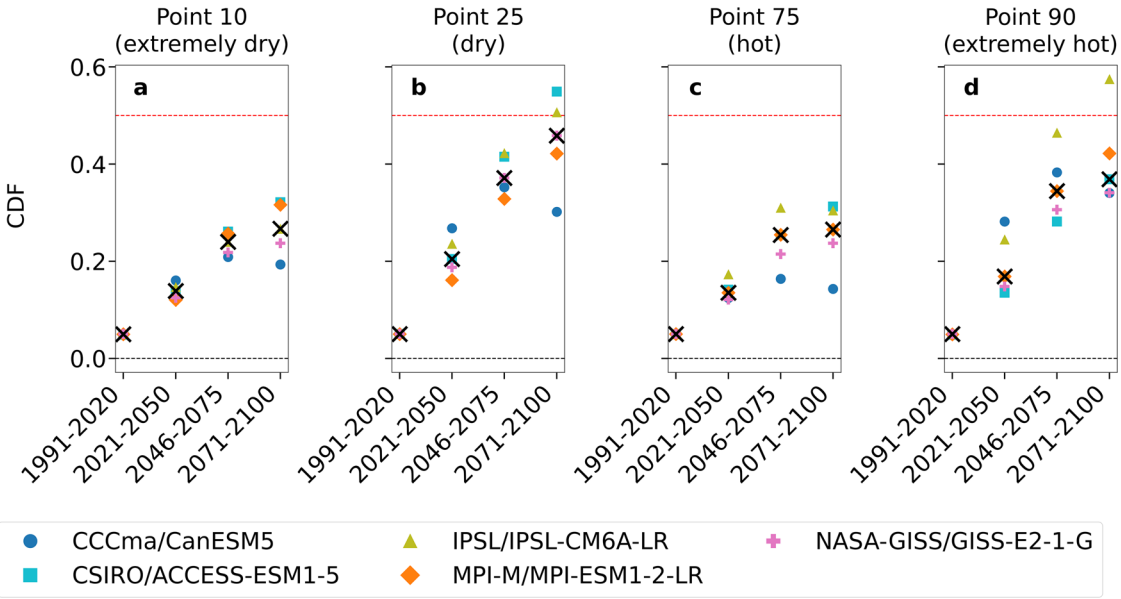

Fig. 8 | Increase in frequency of the four hot and dry reference events during the twenty-first century. Evolution of the joint probability of Point 10 (extremely dry) (**a**), Point 25 (dry) (**b**), Point 75 (hot) (**c**) and Point 90 (extremely hot) (**d**) in August under SSP2-4.5 scenario. The black crosses represent the medians of the five models and the coloured dots each individual model. The horizontal red dashed line represents a cumulative probability of 0.5.

the extreme event defined during the reference period (1991–2020), which previously had only a 4% probability (1 in 25) of occurrence. Again, uncertainties increase with time. In August under SSP5-8.5 scenario, the MPI-ESM1-2-LR model estimates that 66% of the events could be hotter and dryer than the reference extreme event, while the ACCESS-ESM1-5 and GISS-E2-1-G models project a probability of 46%. These results highlight the strong benefits of reducing greenhouse gases emissions to limit the danger of wildfire. They also underscore the importance of swiftly implementing adaptation measures, as even in the lowest emission scenario, the danger from long-term dry conditions increases.

Seasonal danger projection based on joint probability

We now define another hot and dry reference event with SM6-T3-VPD3 based on its joint probability instead of the marginal probabilities of its three components. For instance, with ERA5 data, we estimate a joint probability of 0.05 that a drier and hotter event than August 2022 would occur in Southwestern France. Summer 2022 represents an extreme wildfire season. Therefore, we analyse how an event of such joint probability could evolve with climate change. However, there are multiple triplet of values (*SM6*, *T3*, *VPD3*) that yield a joint probability of 0.05. We defined four reference triplets of values yielding a joint probability of 0.05 in 1991–2020 to assess their evolution over the twenty-first century: Point 10 (extremely dry) (the marginal cumulative probability of SM6 is 0.10), Point 25 (dry) (the marginal cumulative probability of SM6 is 0.25), Point 75 (hot) (the marginal cumulative probabilities of T3 and VPD3 are 0.75) and Point 90 (extremely hot) (the marginal cumulative probabilities of T3 and VPD3 are 0.90) (see "Methods" for details).

The analysis of the evolution of these four reference extreme events reveals that the change in frequency over time varies across the four points. In nearly all cases, including both months, all three climate scenarios, and the five models, Point 25 (dry) and Point 90 (extremely hot) demonstrate the greatest increase in joint probability (see Fig. 8). By the end of the century, in August under SSP2-4.5 scenario, the median probabilities of Point 25 (dry) and Point 90 (extremely hot) across the five models reach 0.46 and 0.37, respectively, with some models exceeding a probability of 0.5, while the joint probabilities of Point 10 (extremely dry) and Point 75 (hot) both reach 0.25

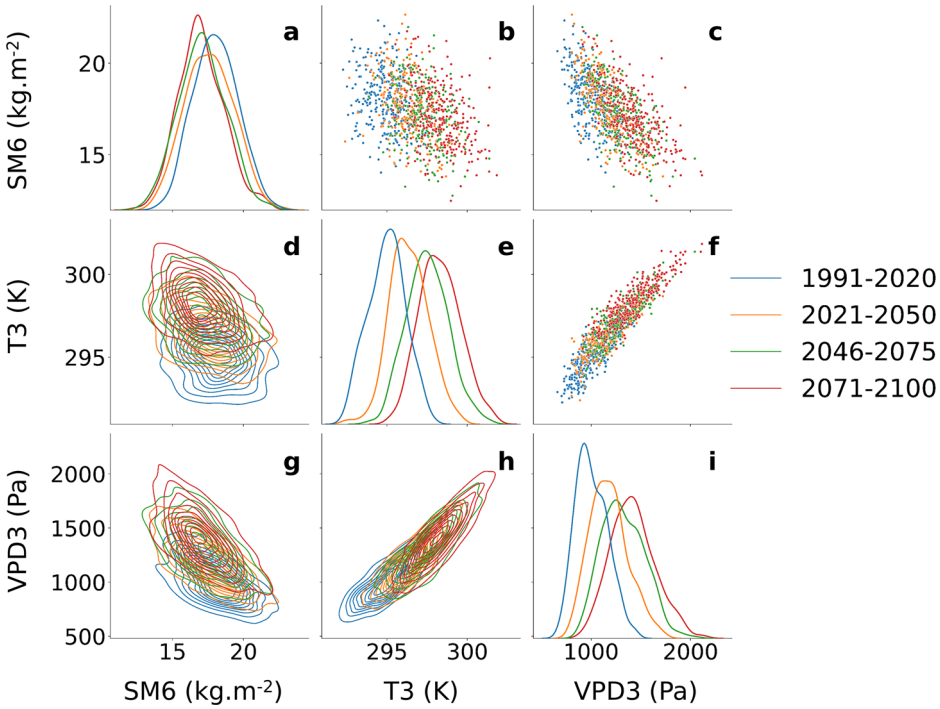

Fig. 9 | Evolution of the marginal and bivariate distributions during the twenty-first century. Marginal distribution of SM6 (**a**), T3 (**e**), and VPD3 (**i**) in the four time periods in August under SSP2-4.5 scenario in the IPSL-CM6A-LR model. Bivariate distributions (**d**, **g**, **h**) and associated data points (**b**, **c**, **f**).

(see Fig. S7 in Supplementary Material for results in July). Several elements can explain this difference. Point 25 (dry) and Point 90 (extremely hot) usually have the highest T3 and VPD3 marginal cumulative probabilities (see Table S1 in Supplementary Material). Investigating the bivariate probability distributions of the studied variables suggests that the change in frequency of compound extreme events is mainly driven by the change in temperature and VPD marginal distributions, and less by soil moisture evolution. Figure 9 shows the bivariate distributions for the IPSL-CM6A-LR model. The four other climate models show similar patterns. On average over the five models, between the two periods 1991–2020 and 2071–2100, the mean SM6 decreases by 0.68 standard deviation in August under SSP2-4.5 scenario, while mean T3 and VPD3 increase by 2.52 and 2.08 standard deviations respectively (see Table S2 in Supplementary Materials for details on each five models). Figure 10 focuses on the four reference points and allows us to compare the evolution over time of the position of the four reference events in the joint trivariate probability distribution. It confirms, as could be suspected when analysing Fig. 9, that their evolution is more influenced by the change in the T3 marginal distribution than by that of SM6. Figure 10 shows the distribution for the IPSL-CM6A-LR model. The four other climate models show similar patterns.

In the climate impact literature, bias-correcting model data is common. The quantile mapping technique has been widely applied when analysing a single climate variable. It consists in finding in the model the event whose cumulative probability would be equal to the one of the studied event in the observations. In the case of compound events, such approach cannot be adopted as an infinite number of triplets of values (in the case of a trivariate distribution) result in the same joint probability. It is rarely possible to find data in the model that have both the same joint probability and marginal probabilities as an event in the observations, as models are not exact representations of the reality. Several multivariate bias correction techniques have emerged recently to tackle this issue, each one providing potentially different outcome as they are based on different mathematical approaches and on the assumption of inter-variable relationships. Our analysis of four reference events provides complementary results to such bias-correction techniques, since it actually reveals the uncertainty or reliability attached to the projection. This methodology we applied to prolonged hot and dry conditions could be used to analyse other compound extreme events.

Inter-comparison across the projections

For the two months and the three scenarios, the increase in probability of extreme conditions prone to wildfires is more pronounced with the seasonal compound index. For instance, under RCP4.5 scenario in July, using the 75th percentile to define the reference event, the probability of the $SM6_{25}$-$T3_{75}$-$VPD3_{75}$ rises from 0.12 to 0.45, while the probability of the FWI_{75} increases from 0.23 to 0.35. Under RCP8.5 scenario in August, using the 90th percentile to define the reference event, the probability of the $SM6_{10}$-$T3_{90}$-$VPD3_{90}$ rises from 0.04 to 0.49, while the probability of the FWI_{90} increases from 0.11 to 0.29. The events analysed with these two indices are different as the reference event defined with the seasonal compound index is rarer than the reference event defined with the FWI_{90}. A complementary analysis (see Fig. S8) indicates that a similar event—defined here by the 95th percentile of the FWI (FWI_{95})—would experience an increase in probability from 0.06 to 0.15 in August under RCP8.5 scenario, representing a substantially more moderate change compared to the event defined by the $SM6_{10}$-$T3_{90}$-$VPD3_{90}$. In addition, the two indices capture events on different timescales. Although the FWI incorporates long-term components (e.g., the DC), it predominantly reflects short-term conditions, particularly through the ISI (see Figs. S1 and S2). In contrast, the SM6-T3-VPD3 index is designed to represent exclusively seasonal conditions, integrating data over periods of up to six months. As such, the results obtained from SM6-T3-VPD3 and the FWI are complementary. They show that seasonal compound hot and dry conditions might increase sharply, which must be considered carefully as compound events often lead to severe impacts[87], while daily fire-weather anomalies are also becoming more frequent. With both indices, under the SSP5-8.5 (RCP8.5) scenario the probability seems to increase more sharply in the second part of the twenty-first century. Under the SSP1-2.6 (RCP2.6) scenario however, the evolution pattern differs as the wildfire danger, as defined with the FWI, might slightly decrease, whereas the likelihood of compound hot and dry conditions increases. This can be due to the fact that the events analysed with the two indices are different, and therefore not fully comparable. It might also result from the slight difference between the scenario used as the FWI projections are based on RCPs designed for CMIP5, while the compound event analysis is based on SSPs from CMIP6. In addition, models used differ between the two analyses. The compound event analysis relies on global climate models (GCM), while the

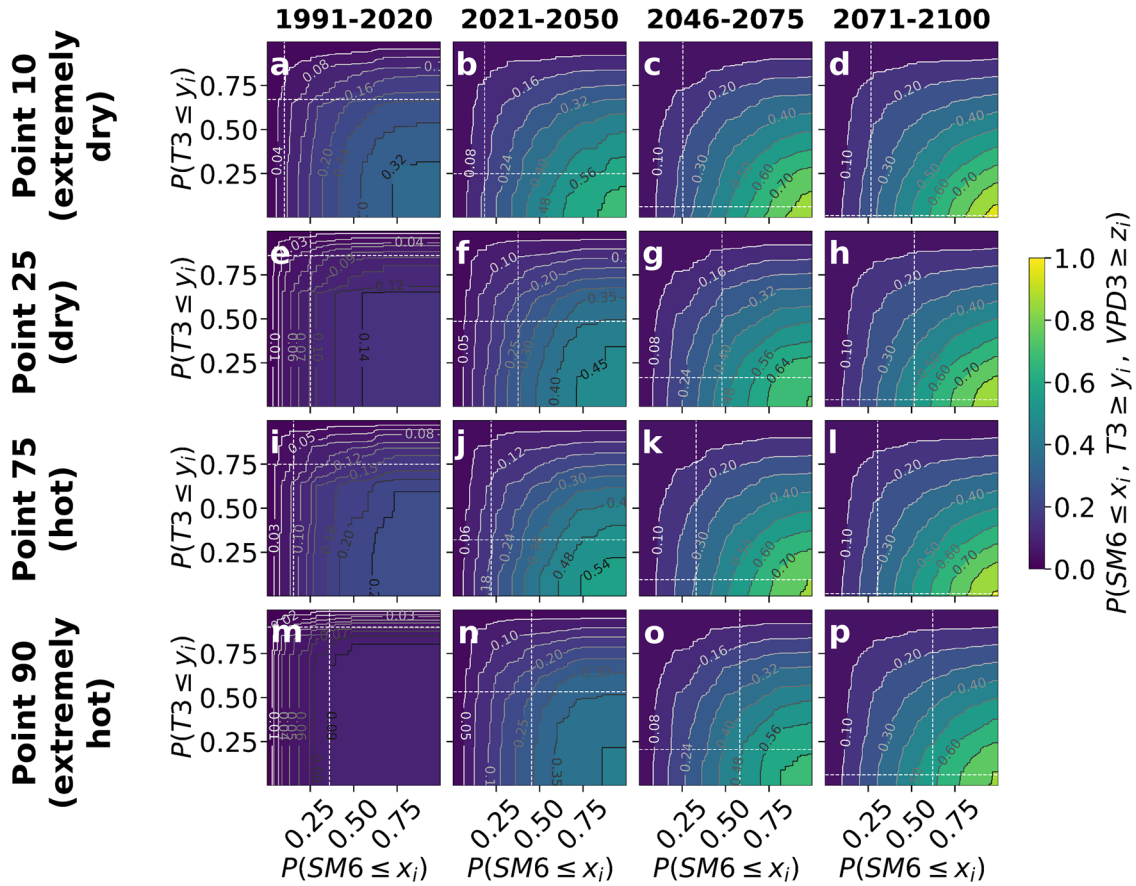

Fig. 10 | Evolution of the joint probability of the four hot and dry reference events during the twenty-first century. The intersections of the white dashed lines represent the joint probabilities of the four reference events. Each row corresponds to one of the four points: **a**–**d**, **e**–**h**, **i**–**l**, and **m**–**p** represent Point 10, 25, 75, and 90, respectively. Each column represents a different time period: **a**, **e**, **i**, **m** correspond to 1991–2020; **b**, **f**, **j**, **n** to 2021−2050; **c**, **g**, **k**, **o** to 2046–2075; and **d**, **h**, **l**, **p** to 2071–2100. All data refer to August under the SSP2-4.5 scenario using the IPSL-CM6A-LR model. The coloured background and the isolines represent the joint probability distribution. The joint probability distribution is in three dimensions. So each panel represents the joint probability distribution in a plane corresponding to a given marginal probability of VPD3, equal to the one of T3 for the reference event considered.

FWI analysis relies on a regional climate model (RCM) nested into a GCM. The studied domain is located in a transition area between the Mediterranean region that is expected to become warmer and drier with climate change, and North-western Europe expected to become wetter[88]. This could induce variability across models.

A complementary analysis was conducted to compare SM6-T3-VPD3 with the accumulated version of the FWI through the Daily Severity Rating (DSR) (see Methods). Specifically, DSR1, DSR3, and DSR6 were calculated using ERA5 data from 2003 to 2022 by accumulating daily DSR values over 1, 3, and 6 months, respectively. The correlation between SM6-T3-VPD3 and these accumulated DSR indices was moderate, with Kendall correlation coefficients of 0.30, 0.46, and 0.49 for DSR1, DSR3, and DSR6, respectively (see Fig. S2). DSR3 and DSR6 are strongly correlated with one another, likely because DSR emphasises high FWI values, which predominantly occur during summer. As a result, although DSR6 includes spring values, these may be dominated by the more extreme summer conditions. This suggests that DSR6 may not effectively capture the potential influence of spring drought on wildfire danger.

In a second step, we analysed projections of the 95th percentile of DSR1, DSR3, and DSR6—referred to as $DSR1_{95}$, $DSR3_{95}$, and $DSR6_{95}$—under the three climate scenarios (see Figs. S9–S11), in order to compare them with FWI_{95} and $SM6_{10}$-$T3_{90}$-$VPD3_{90}$. As expected, DSR3 and DSR6 show similar projected trends, consistent with their strong correlation. The projected increases in $DSR3_{95}$ and $DSR6_{95}$ are more pronounced than those of FWI_{95} (Fig. S8), but remain more moderate compared to the stronger increases projected for $SM6_{10}$-$T3_{90}$-$VPD3_{90}$ (Fig. 7).

Discussion

In its last report, the IPCC Working Group II underlined a lack of robust wildfires incidences and magnitudes assessment in Europe[10]. In this article, we try to remediate the issue with two complementary indices based respectively on the seasonal compound dry and hot conditions and the daily variations of the fire-weather. The aim of this study was to evaluate the evolution of the two primary factors that control the extent of burnt area defined by Pereira et al.[69], the long-term "climate anomalies" and the short-term "weather anomalies". Both indices estimate a strong increase in the wildfire danger. Results demonstrate the benefit of limiting greenhouse gas emissions as the probability of compound hot and dry conditions is of 0.15 under SSP1-2.6 scenario, but reaches 0.49 under SSP5-8.5 scenario in August at the end of the century. Meanwhile, the probability of occurrence of extreme fire-weather, as characterised by FWI_{90}, is rising from 0.11 to 0.29 in August under RCP8.5 scenario, whereas it might slightly decrease under RCP2.6 scenario. It also advocates for adaptation measures, as all models and all indices reveal an increase in the likelihood of climate conditions prone to wildfires (except the FWI under RCP2.6 scenario). In particular, according to the seasonal compound index, the sharpest increase might occur during the first half of the century, meaning that adaptation measures to face the increase in wildfire danger need to be developed as of today. In addition, uncertainties are wider at the end of the century, meaning that in the worst case, the frequency of extreme conditions could be even higher than stated previously (see Fig. 5). If local authorities are willing to prepare for the worst-case scenario, they should consider the upper bound of the confidence interval. For instance, the 2022 wildfire season in Southwestern

France, which resulted in over 30,000 hectares burned, was associated with exceptionally hot and dry conditions—as indicated by the SM6-T3-VPD3 index—whose estimated likelihood was 0.05 (1 in 20). Under the RCP4.5 climate change scenario, the probability of such an event could increase to 0.57 (see Fig. 5b).

We carried out our analysis for each month independently as our aim is to investigate how monthly conditions will diverge from mean conditions for each month. Indeed, each month features specific environmental conditions (phenological stage, vegetation dryness) and socio-economic context (e.g. level of touristic frequentation of the forest). From an adaptation point of view, it might be useful for local stakeholders and decision-makers to think in terms of a monthly frame of reference. In addition, we showed that to analyse the evolution of risks associated with compound events, it is relevant to analyse a set of points having different marginal probabilities as the intervariable relationships evolve with climate change. By analysing four reference points (two more related to temperature extremes, and two others to soil moisture extremes), we showed that a single joint probability can represent multiple compound conditions and that the frequency of each will evolve differently under climate change. This methodology could be applied to other compound events.

Hetzer et al.[56] analysed the evolution of the value of the 95th percentile of FWI in Europe. This means they fixed a probability and analysed how does the corresponding value of the FWI evolve, whereas we fixed the intensity and analysed how its probability evolves. Decision-makers are better able to address risks associated with familiar events[89]. Therefore, defining reference events on the past period and assessing their likelihood on short-term, medium-term and long-term period in different scenarios is of significant interest. It should help local decision-makers foresee the evolution of the wildfire risk and develop adaptation strategies. It also makes the methodology we developed easily applicable to other regions. The 90th percentile of the FWI (FWI_{90}) used in this study corresponds to fire-weather conditions similar to those observed on 6 August 2022—3 days prior to the onset of the "Landiras 2" wildfire. Likewise, the conditions associated with a joint probability of 0.05, as defined by the SM6-T3-VPD3 index, reflect the exceptional meteorological extremes experienced during the summer of 2022. Hetzer et al.[56] focused on 1950–2080 and used different models. Therefore, results are not easily comparable. Nevertheless, they are coherent as Hetzer et al.[56] also found a sharp increase in fire-weather, especially in the SSP5-8.5, as we did. Bedia et al.[55] used the A1B emission scenario, corresponding to an intermediate level between RCP4.5 and RCP8.5[90]. They analysed the frequency-over-threshold 30 (FOT30) defined as the number of days with FWI greater than 30. In France, they found that the FOT30 approximately increases from 10% to 25% between 1971–2000 and 2071–2100. Again, although not directly comparable, the results of Bedia et al.[55] are coherent with our results, as the reference event we defined with the 90th percentile of FWI on 1991–2020 is close to 30 (see Table S3 in Supplementary Material). Fargeon et al.[91] also analysed the evolution of FOT30 under RCP4.5 and RCP8.5 scenarios. They focused on the wildfire danger at national level, not Southwestern France specifically. Nevertheless, as in our analysis, they found a much steeper increase under RCP8.5 compared to RCP4.5 after 2050.

No other study has analysed hot and dry compound events using indicators combining temperature, soil moisture and VPD on different timescales. However, several studies have analysed them using temperature and precipitation. In particular, Dosio et al.[92] studied the evolution of record-breaking and unprecedented compound hot and dry summers in Europe. As we did, they found that even under a low-emission scenario (RCP2.6), model projections indicate a probable rise in the frequency of compound hot and dry events by the end of the century. Felsche et al.[93] analysed European hot and dry summers focussing on temperature and precipitation. They found that in the Atlantic coast region, that encompasses our study area, the likelihood of an extreme hot and dry summer like the one of 2003 will increase from 0.001 in the present climate (2001–2022) to 0.36 at a Global Warming Level (GWL) of +3 °C compared to 1850–1900. Our methodology is different so our results are not directly comparable to this study, however Point 90 (extremely hot), closest to that analysed by Felsche et al. (a hot but moderately dry event) shows a similar increase from 0.05 to 0.36 in SSP2-4.5 by the end of the century. Finally, a number of studies have investigated future changes in short- to long-term droughts (1-, 3-, and 12-month durations) across the Mediterranean Basin, reporting a robust increase in drought frequency under climate change scenarios[94–96].

The methodology developed in this study could be adapted and applied to regions with similar wildfire regimes. The use of percentiles based on a reference period enables analyses that are tailored to local conditions. If necessary, the variables and timescales incorporated into the seasonal compound index can be adjusted to better suit different regional contexts. In all cases, however, the application of the index in a new context would require prior validation. Particular caution is warranted in fuel-limited environments, where fuel accumulation, rather than weather conditions, is the primary driver of fire risk[97]. Other impacts of climate change could also be analysed using this methodology, such as agricultural droughts. In addition, the methodology we developed to analyse a compound event by fixing either the marginal probabilities or the joint probability allows us to better understand and characterise the evolution of the compound event and the relations between variables.

To bring this analysis further, it would be interesting to analyse the FWI with a larger set of simulations to better assess uncertainties (C3S provides three simulations, only one of which was evaluated as satisfactory for our analysis). It would also be of interest to analyse the evolution of pyroconvective risk. Pyroconvective phenomena have been implicated in several recent extreme wildfires, producing hazardous and unpredictable fire behaviour[30,61,98–100]. Owing to their projected increase in frequency under climate change, such events are expected to pose an additional challenge for firefighting operations[101,102]. In addition, this study focused exclusively on July and August, despite the fact that wildfires also occur during other seasons. A comprehensive analysis of the climate–fire relationship across the entire year is necessary to identify which indices are most relevant for assessing the evolution of wildfire danger beyond the summer months. In Southwestern France, the drivers and dynamics of spring and autumn wildfires differ substantially from those in summer and are therefore beyond the scope of this study. As such, the seasonal compound index employed here may not be suitable for analysing spring and autumn wildfires, nor for evaluating a potential extension of the wildfire season, as explored in other studies conducted in France and the broader Mediterranean region[57,103,104]. In this article, we focused on the climate drivers of wildfire. To refine the risk projection, other drivers should be investigated, such as fire-vegetation feedbacks and human-related factors on the climate-fire relationship[57]. For instance, population has been increasing in the Landes forest in the last few years[105], which increases the exposure to the wildfire risk.

Evolution in fire danger due to climate change is of strong concern, as extreme hot and dry events on the reference period might become normal conditions at the end of the century. This poses serious threats to the region as wildfires have multiple environmental and socio-economic impacts. Previous studies revealed increasing risks in neighbouring countries[50,51,53,55,56,106]. While international cooperation in wildfire response is routinely activated during extreme events, the increasing likelihood of simultaneous wildfires across multiple European countries may strain shared resources, highlighting the need for stronger inter-agency coordination and deeper integration at the regional level.

Adapting to the escalating risk of wildfires necessitates a comprehensive approach that addresses the three fundamental components of risk: danger (also referred as hazard), exposure, and vulnerability[10,46]. Mitigating the hazard involves decreasing the likelihood and potential severity of wildfire events. This can be achieved through public education campaigns that promote fire-safe behaviours among residents, tourists, and professionals. Fuel management practices, such as prescribed burning and mechanical thinning, have proven effective in reducing wildfire severity[107]. Exposure can be curtailed by regulating the expansion of human settlements and infrastructure into fire-prone areas, particularly the wildland–urban interface (WUI). The WUI, where human development meets undeveloped

wildland, has been identified as a zone of heightened wildfire risk. Efforts to limit development in these areas can reduce the number of structures and lives at risk[108–110]. However, it is important to recognise that even without further expansion, existing exposure within the WUI remains substantial. Moreover, many peri-urban areas—often overlapping with the WUI—provide essential affordable housing, underscoring the need to balance wildfire risk reduction with broader social and economic considerations[111]. Finally, reducing vulnerability entails enhancing the resilience of communities and systems to withstand and recover from wildfire events. This includes bolstering firefighting capacities, implementing early warning systems, refining evacuation procedures, retrofitting properties in the WUI to resist fire hazards, creating funding mechanisms to support adaptation and developing specialised insurance schemes and healthcare plans tailored to wildfire-related emergencies[112–114]. By systematically addressing hazard, exposure, and vulnerability, these strategies collectively contribute to a more resilient approach to managing the increasing threat of wildfires in the context of climate change. However, for such adaptation strategy to be effective, all the stakeholders involved need to collaborate (individual property owners, local decision makers, government agencies, etc.)[115,116].

Methods

Data to compute the seasonal compound index

Monthly mean soil moisture, surface air temperature, pressure, relative humidity and specific humidity are analysed using five climate models from the 6th Coupled Model Intercomparison Project (CMIP6): ACCESS-ESM1.5, CanESM5, GISS-E2.1-G, IPSL-CM6A-LR and MPI-ESM1.2-LR. Historical simulations and three Shared Socioeconomic Pathways (SSP) are analysed: SSP1-2.6, SSP2-4.5, SSP5-8.5 (see Table S4 in Supplementary Materials for details on the models and the simulations used). These three scenarios are studied to reflect the range of uncertainty on the future global warming levels. SSP1-2.6 is the lowest emission scenario, in which global warming is kept below +2 °C, the limit set in the Paris Agreement. SSP5-8.5 is the highest emission scenario, in which global warming reaches around +5 °C by 2100. SSP2-4.5, often referred to as "business as usual", represents a medium scenario in which global warming reaches more than +2.5 °C by 2100, and reflects current policies better than SSP1-2.6[117–119].

VPD is defined as the difference between the saturated water vapour pressure (e_s, Pa) and the actual one (e, Pa), and calculated with the following formula:

$$\mathrm{VPD} = e_s - e = \frac{q_s}{\varepsilon + (1-\varepsilon)q_s} P - \frac{q}{\varepsilon + (1-\varepsilon)q} P \quad (1)$$

Where q_s and q are the surface air saturated and actual specific humidity in kg/kg, P the surface atmospheric pressure in Pa, and ε is the ratio of the molecular weight of water vapour to the molecular weight of dry air ($\varepsilon = 0.622$). q_s is computed as $q_s = \frac{q}{\left(\frac{RH}{100}\right)}$, where RH is the relative humidity in %.

FWI data

The Fire Weather Index (FWI) is an indicator of weather conditions favourable for wildfires. There is a standard computation methodology[47]. The input variables are daily noon values of air temperature, relative humidity, wind speed and 24-h accumulated precipitation. But the FWI is not directly available in global climate models, and the input variables necessary to apply the standard computation methodology are rarely provided. They are however available through a certain number of CORDEX regional climate simulations. In this article, we used FWI projections from the Copernicus Climate Change Service (C3S). The output from three GCM/RCM pairs, developed within the EURO-CORDEX[120] are evaluated: ICHEC-EC-EARTH/RCA4, MPI-M-MPI-ESM-LR/RCA4 and MOHC-HadGEM2-ES/RCA4, the Swedish Rossby Center Atmospheric model version 4 (RCA4)[121] being nested into three global models, EC-Earth[122], MPI-ESM[123] (Max-Planck Institute) and HadGEM[124] (UK Met Office). Three Representative Concentration Pathways (RCP) are analysed: RCP2.6, RCP4.5 and RCP8.5.

ERA5 and models' data are interpolated on the domain lying between −1.25° and 1.25° in longitude, and 43.73° N and 45° N in latitude.

Daily wildfire danger analysis

A reference extreme event is defined using the 90th percentile of the FWI (FWI_{90}) on 1991–2020 for July and August respectively, under RCP4.5 scenario. A cumulative density function (CDF) is fitted to the data to estimate the probability of occurrence of such an event on four periods: the reference (1991–2020), short-term (2021–2050), medium-term (2046–2075), and long-term (2071–2100) period. The same analysis is conducted using the 75th percentile of the FWI (FWI_{75}) to assess the effect of defining a less extreme reference event. Finally, we assessed the evolution of the 90th percentile of the FWI under RCP2.6 and RCP8.5 scenarios to compare the evolution of the danger in different emission scenarios. We study the survival probability (1 − CDF) to ease the comparison with the seasonal compound index analysis.

Uncertainties on the results are assessed by bootstrapping. For each month and each four periods studied, 1000 samples are created. The probability of the FWI is computed, with a 95% confidence interval.

Daily Severity Rating (DSR)

The Daily Severity Rating (DSR) and its averaged form over a season, the Seasonal Severity Rating (SSR), are both indicators derived from the Fire Weather Index (FWI) system. The DSR applies a non-linear transformation to daily FWI values, typically using a power-based function: $\mathrm{DSR} = 0.0272 \times \mathrm{FWI}^{1.77}$

This formulation amplifies the influence of higher FWI values, highlighting days with particularly severe fire weather conditions[47]. When aggregated over time, the DSR provides a cumulative measure of fire potential, offering insight into the persistence and intensity of hazardous conditions throughout a given period. In the current study, we accumulate DSR over 1, 3 and 6 months, producing DSR1, DSR3 and DSR6.

FWI projections' evaluation

The three FWI projections provided by C3S are evaluated against ERA5 data. We analyse the changes in the CDF of a reference event, defined as the 90th (75th) percentile for 1991–2020, between the periods 1970–1999 and 1991–2020 under RCP4.5 scenario, considering both July and August. Only one model shows trends close to the one assessed with ERA5 (see Figs. S12 and S13 in Supplementary Materials). Therefore, only the MPI-ESM-LR/RC4 simulation is used to perform our analysis.

Seasonal wildfire danger analysis

The empirical joint probability of a hot and dry event is assessed using the Gringorten plotting position formula in the trivariate case[125–127], following Eq. (2):

$$P(\mathrm{SM6} \le x_i, \mathrm{T3} \ge y_j, \mathrm{VDP3} \ge z_k) = \frac{m - 0.44}{n + 0.12} \quad (2)$$

Where n is the number of data points and m is the number of data points verifying the condition ($\mathrm{SM6} \le x_i$ and $\mathrm{T3} \ge y_j$ and $\mathrm{VDP3} \ge z_k$) with $1 \le i, j, k \le n$. SM6 is computed by integrating soil moisture over 6 months, so for instance, the value of SM6 in August is the integration of soil moisture from March to August. $T3$ (VPD3) is computed by integrating temperature (VPD) over 3 months, so for instance, the value of $T3$ (VPD3) in August is the integration of temperature (VPD) from June to August. This empirical joint probability is computed in July and August, the two summer months analysed in this study. In contrast to Lanet et al.[21], we do not apply the inverse cumulative distribution function of the normal distribution to standardise the data, as this approach is not suitable for analysing the more than 100-year period under study, during which the climate is no more stationary.

Lanet et al.[21] evaluated multiple combinations of integration periods. In the present study, we selected three additional indices—SM6-T3-VPD1, SM3-T3-VPD3, and SM1-T1-VPD1—that exhibited comparable performance to SM6-T3-VPD3 in predicting burnt area, in order to conduct a sensitivity analysis on the index used for projecting wildfire danger.

VPD can exhibit a strong response to temperature[79]. However, climate change may alter the intervariable relationship between temperature and VPD, as has been observed for other variables[128]. Figure S14 illustrates that during the twenty-first century, the temperature distribution shifts toward higher values without a change in its distribution shape (panel e), whereas the VPD distribution becomes wider, with an extended right tail corresponding to higher VPD values (panel i). This divergence leads to a change in the intervariable relationship (panel h). The empirical joint cumulative probability computed using Eq. (2) is based on a copula method, which allows us to capture the dependence among the three variables that constitute the index.

The reference compound extreme event is defined in two different ways. First, it is defined by combining the 10th (25th) percentile of SM6, and the 90th (75th) percentile of T3 and VPD3 on 1991–2020. As for the FWI analysis, the joint probability of this reference event is assessed on four periods (1991–2020, 2021–2050, 2046–2075, and 2071–2100), pooling together all the simulations used into one large distribution for each model (ten ensemble members are used in the case of SSP2-4.5, and five in the case of SSP1-2.6 and SSP5-8.5). This analysis is performed on July and August and using the five climate models independently.

Afterwards, we define a reference event by setting the joint probability instead of the marginal probabilities. We choose a joint probability of 0.05 as it is the value we assess for August 2022 with ERA5 data. In addition, we set the constraint that the marginal probability of T3 ($P(T3 \le y_i)$) is equal to the marginal probability of VDP3 ($P(\mathrm{VPD3} \le \mathrm{z_i})$) for a given event characterised by $\mathrm{SM6} = \mathrm{x_i}$ and $T3 = y_i$ and $\mathrm{VPD3} = \mathrm{z_i}$ to decrease the dimensionality of the problem. We select four reference events corresponding to four points in the joint-probability chart. Two of them are more related to temperature extremes, and two others to soil moisture extremes. The first point (noted as Point 10 (extremely dry)) is defined by setting $P(\mathrm{SM6} \le \mathrm{x_i}) = 0.1$, the second (Point 25 (dry)) $P(\mathrm{SM6} \le \mathrm{x_i}) = 0.25$, the third (Point 75 (hot)) $P(T3 \le y_i) = 0.75$ and the fourth (Point 90 (extremely hot)) $P(T3 \le y_i) = 0.90$. The joint probabilities of these four reference events defined on 1991–2020 are then assessed for three other periods, 2021–2050, 2046–2075, and 2071–2100, under three emission scenarios, in July and August and for each five global climate models.

CMIP6 models' evaluation

The objective of this models' evaluation is to compare the joint relation between the three climate variables in the models and in ERA5 data in the case of extreme hot and dry events. In this article, we performed two different analyses, fixing either the marginal probabilities of the three climate variables or the joint probability of four points. Therefore, we performed two different models' evaluation. First, we assessed the empirical joint probability of a compound event defined on 1991–2020 as the combination of the 10th (25th) percentile of SM6, and the 90th (75th) percentile of both T3 and VPD3 for July and August using ERA5 data and each ten simulations of the five climate models (using historical simulations for 1991–2014 and SSP2-4.5 for 2015–2020). The empirical joint probability computed from ERA5 data is in the range of empirical joint probabilities computed with the ensemble members of each model. Therefore, the five climate models are considered satisfactory for the first analysis conducted in this article (see Figs. S15 and S16 in Supplementary Materials). Then, we fixed a joint probability of 0.05, and we set the constraint $P(T3 \le y_i) = P(\mathrm{VPD3} \le \mathrm{z_i})$. For Points 10 (extremely dry) and 25 (dry), we set $P(\mathrm{SM6} \le \mathrm{x_i}) = 0.1$ and $P(\mathrm{SM6} \le \mathrm{x_i}) = 0.25$, respectively. Therefore, to evaluate the model, we compared the marginal probability of T3 ($P(T3 \le y_i)_{\mathrm{Point10}}$ and $P(T3 \le y_i)_{\mathrm{Point25}}$) in ERA5 to the ones in the ten ensemble members of each model (see Table S4 in Supplementary Materials for the climate models and simulations used). For Points 75 (hot) and 90 (extremely hot), we set $P(T3 \le y_i) = 0.75$ and $P(T3 \le y_i) = 0.90$, respectively. Therefore, to evaluate the model, we compared the marginal probability of SM6 ($P(\mathrm{SM6} \le \mathrm{x_i})_{\mathrm{Point75}}$ and $P(\mathrm{SM6} \le \mathrm{x_i})_{\mathrm{Point90}}$). In most cases (for the four points and the 2 months), the marginal probability computed from ERA5 data is in the range of marginal probabilities computed with the ensemble members of each model. Therefore, the five climate models are considered satisfactory for the second analysis conducted in this article (see Figs. S17–S20 in Supplementary Materials).

Data availability

CMIP6 data are publicly available through the Earth System Grid Federation (https://esgf-node.llnl.gov/search/cmip6/), and the FWI projections through Copernicus Climate Change Service (C3S) Climate Data Store (CDS) (https://doi.org/10.24381/cds.ca755de7). ERA5 data are also publicly available through the Climate Data Store (https://cds.climate.copernicus.eu/cdsapp#!/dataset/reanalysis-era5-pressure-levels?tab=overview), as well as the ESA Climate Change Initiative Land Cover (https://cds.climate.copernicus.eu/datasets/satellite-land-cover?tab=overview) (https://doi.org/10.24381/cds.006f2c9a). The BDIFF burnt area French database is publicly available through https://bdiff.agriculture.gouv.fr/.

Received: 20 April 2025; Accepted: 9 July 2025;
Published online: 23 July 2025

References

1. Tedim, F. et al. Defining extreme wildfire events: difficulties, challenges, and impacts. *Fire* **1**, 9 (2018).
2. Hu, Y., Yue, X. & Tian, C. Climatic drivers of the Canadian wildfire episode in 2023. *Atmos. Ocean Sci. Lett.* **17**, 100483 (2024).
3. Jain, P. et al. Drivers and impacts of the record-breaking 2023 wildfire season in Canada. *Nat. Commun.* **15**, 6764 (2024).
4. Erni, S. et al. Mapping wildfire hazard, vulnerability, and risk to Canadian communities. *Int. J. Disaster Risk Reduct.* **101**, 104221 (2024).
5. Whittaker, J., Haynes, K., Handmer, J. & McLennan, J. Community safety during the 2009 Australian 'Black Saturday' bushfires: an analysis of household preparedness and response. *Int. J. Wildland Fire* **22**, 841–849 (2013).
6. Kala, J., Evans, J. P. & Pitman, A. J. Influence of antecedent soil moisture conditions on the synoptic meteorology of the Black Saturday bushfire event in southeast Australia. *Q. J. R. Meteorol. Soc.* **141**, 3118–3129 (2015).
7. Engel, C. B., Lane, T. P., Reeder, M. J. & Rezny, M. The meteorology of Black Saturday. *Q. J. R. Meteorol. Soc.* **139**, 585–599 (2013).
8. Boer, M. M., Resco de Dios, V. & Bradstock, R. A. Unprecedented burn area of Australian mega forest fires. *Nat. Clim. Chang.* **10**, 171–172 (2020).
9. Filkov, A. I., Ngo, T., Matthews, S., Telfer, S. & Penman, T. D. Impact of Australia's catastrophic 2019/20 bushfire season on communities and environment. Retrospective analysis and current trends. *J. Saf. Sci. Resil.* **1**, 44–56 (2020).
10. IPCC. *Climate Change 2022—Impacts, Adaptation and Vulnerability: Working Group II Contribution to the Sixth Assessment Report of the Intergovernmental Panel on Climate Change*. (Cambridge University Press, 2023).
11. Mills, G. et al. Meteorological drivers of the eastern Victorian Black Summer (2019–2020) fires. *J. South. Hemisph. Earth Syst. Sci.* **72**, 139–163 (2022).
12. Cai, D., Abram, N. J., Sharples, J. J. & Perkins-Kirkpatrick, S. E. Increasing intensity and frequency of cold fronts contributed to Australia's 2019–2020 Black Summer fire disaster. *Environ. Res. Lett.* **17**, 094044 (2022).
13. Udy, D. G., Vance, T. R., Kiem, A. S., Holbrook, N. J. & Abram, N. Australia's 2019/20 Black Summer fire weather exceptionally rare over the last 2000 years. *Commun. Earth Environ.* **5**, 1–13 (2024).

14. Suppression, U.S. Department of the Interior. U.S. Department of the Interior https://www.doi.gov/wildlandfire/suppression (2025).
15. San-Miguel-Ayanz, J. et al. Forest Fires in Europe, Middle East and North Africa 2017. https://publications.jrc.ec.europa.eu/repository/handle/JRC112831 (2018).
16. Turco, M. et al. Climate drivers of the 2017 devastating fires in Portugal. *Sci. Rep.* **9**, 13886 (2019).
17. San-Miguel-Ayanz, J. et al. Forest Fires in Europe, Middle East and North Africa 2018. https://publications.jrc.ec.europa.eu/repository/handle/JRC117883 (2019).
18. Papathoma-Köhle, M. et al. A wildfire vulnerability index for buildings. *Sci. Rep.* **12**, 6378 (2022).
19. Masoom, A. et al. Investigation of the effects of the Greek extreme wildfires of August 2021 on air quality and spectral solar irradiance. *Atmos. Chem. Phys.* **23**, 8487–8514 (2023).
20. Rodrigues, M. et al. Drivers and implications of the extreme 2022 wildfire season in Southwest Europe. *Sci. Total Environ.* **859**, 160320 (2023).
21. Lanet, M., Li, L., Ehret, A., Turquety, S. & Le Treut, H. Attribution of summer 2022 extreme wildfire season in Southwest France to anthropogenic climate change. *npj Clim. Atmos. Sci.* **7**, 267 (2024).
22. San-Miguel-Ayanz, J. et al. Forest Fires in Europe, Middle East and North Africa 2023. https://publications.jrc.ec.europa.eu/repository/handle/JRC139704 (2024).
23. Abatzoglou, J. T. & Williams, A. P. Impact of anthropogenic climate change on wildfire across western US forests. *Proc. Natl. Acad. Sci. USA* **113**, 11770–11775 (2016).
24. Barbero, R., Abatzoglou, J. T., Pimont, F., Ruffault, J. & Curt, T. Attributing increases in fire weather to anthropogenic climate change over France. *Front. Earth Sci.* **8**, 104 (2020).
25. Kirchmeier-Young, M. C., Zwiers, F. W., Gillett, N. P. & Cannon, A. J. Attributing extreme fire risk in Western Canada to human emissions. *Clim. Change* **144**, 365–379 (2017).
26. Kirchmeier-Young, M. C., Gillett, N. P., Zwiers, F. W., Cannon, A. J. & Anslow, F. S. Attribution of the influence of human-induced climate change on an extreme fire season. *Earths Future* **7**, 2–10 (2019).
27. Pereira, M. G., Gonçalves, N. & Amraoui, M. The influence of wildfire climate on wildfire incidence: the case of Portugal. *Fire* **7**, 234 (2024).
28. Barnes, C. et al. Climate change made weather conditions leading to deadly South Korean wildfires about twice as likely. World Weather Attribution, 1-55 (2025).
29. Krikken, F., Lehner, F., Haustein, K., Drobyshev, I. & van Oldenborgh, G. J. Attribution of the role of climate change in the forest fires in Sweden 2018. *Nat. Hazards Earth Syst. Sci.* **21**, 2169–2179 (2021).
30. Abram, N. J. et al. Connections of climate change and variability to large and extreme forest fires in southeast Australia. *Commun. Earth Environ.* **2**, 1–17 (2021).
31. Richardson, D. et al. Global increase in wildfire potential from compound fire weather and drought. *npj Clim. Atmos. Sci.* **5**, 1–12 (2022).
32. Jolly, W. M. et al. Climate-induced variations in global wildfire danger from 1979 to 2013. *Nat. Commun.* **6**, 7537 (2015).
33. Turco, M. et al. Exacerbated fires in Mediterranean Europe due to anthropogenic warming projected with non-stationary climate-fire models. *Nat. Commun.* **9**, 3821 (2018).
34. Senande-Rivera, M., Insua-Costa, D. & Miguez-Macho, G. Spatial and temporal expansion of global wildland fire activity in response to climate change. *Nat. Commun.* **13**, 1208 (2022).
35. Archibald, S., Lehmann, C. E. R., Gómez-Dans, J. L. & Bradstock, R. A. Defining pyromes and global syndromes of fire regimes. *Proc. Natl. Acad. Sci. USA* **110**, 6442–6447 (2013).
36. Bradstock, R. A. A biogeographic model of fire regimes in Australia: current and future implications. *Glob. Ecol. Biogeogr.* **19**, 145–158 (2010).
37. Syphard, A. D., Radeloff, V. C., Hawbaker, T. J. & Stewart, S. I. Conservation threats due to human-caused increases in fire frequency in Mediterranean-climate ecosystems. *Conserv. Biol.* **23**, 758–769 (2009).
38. Le Page, Y., Oom, D., Silva, J. M. N., Jönsson, P. & Pereira, J. M. C. Seasonality of vegetation fires as modified by human action: observing the deviation from eco-climatic fire regimes. *Glob. Ecol. Biogeogr.* **19**, 575–588 (2010).
39. Aldersley, A., Murray, S. J. & Cornell, S. E. Global and regional analysis of climate and human drivers of wildfire. *Sci. Total Environ.* **409**, 3472–3481 (2011).
40. Ganteaume, A., Barbero, R., Jappiot, M. & Maillé, E. Understanding future changes to fires in southern Europe and their impacts on the wildland-urban interface. *J. Saf. Sci. Resil.* **2**, 20–29 (2021).
41. Bowman, D. M. J. S. et al. Human exposure and sensitivity to globally extreme wildfire events. *Nat. Ecol. Evol.* **1**, 1–6 (2017).
42. Canadell, J. G. et al. Multi-decadal increase of forest burned area in Australia is linked to climate change. *Nat. Commun.* **12**, 6921 (2021).
43. Fang, L., Yang, J., Zu, J., Li, G. & Zhang, J. Quantifying influences and relative importance of fire weather, topography, and vegetation on fire size and fire severity in a Chinese boreal forest landscape. *For. Ecol. Manag.* **356**, 2–12 (2015).
44. Squire, D. T. et al. Likelihood of unprecedented drought and fire weather during Australia's 2019 megafires. *npj Clim. Atmos. Sci.* **4**, 1–12 (2021).
45. Williams, A. P. et al. Observed impacts of anthropogenic climate change on wildfire in California. *Earths Future* **7**, 892–910 (2019).
46. Chuvieco, E. et al. Towards an integrated approach to wildfire risk assessment: when, where, what and how may the landscapes burn. *Fire* **6**, 215 (2023).
47. Van Wagner, C. E. *Development and Structure of the Canadian Forest Fire Weather Index System*, Forestry Technical Report 35 (Canadian Forestry Service, Headquarters, Ottawa, 1987).
48. Touma, D. Canadian Forest Fire Weather Index (FWI). *NCAR Climate Data Guide* https://climatedataguide.ucar.edu/climate-data/canadian-forest-fire-weather-index-fwi (2023).
49. Wotton, B. M. Interpreting and using outputs from the Canadian Forest Fire Danger Rating System in research applications. *Environ. Ecol. Stat.* **16**, 107–131 (2009).
50. Rovithakis, A. et al. Future climate change impact on wildfire danger over the Mediterranean: the case of Greece. *Environ. Res. Lett.* **17**, 045022 (2022).
51. Faggian, P. Estimating fire danger over Italy in the next decades. *Eur. Mediterr. J. Environ. Integr.* **3**, 15 (2018).
52. Kalabokidis, K. et al. Effect of climate change projections on forest fire behavior and values-at-risk in Southwestern Greece. *Forests* **6**, 2214–2240 (2015).
53. Karali, A. et al. Sensitivity and evaluation of current fire risk and future projections due to climate change: the case study of Greece. *Nat. Hazards Earth Syst. Sci.* **14**, 143–153 (2014).
54. Moriondo, M. et al. Potential impact of climate change on fire risk in the Mediterranean area. *Clim. Res.* **31**, 85–95 (2006).
55. Bedia, J., Herrera, S., Camia, A., Moreno, J. M. & Gutiérrez, J. M. Forest fire danger projections in the Mediterranean using ENSEMBLES regional climate change scenarios. *Clim. Change* **122**, 185–199 (2014).
56. Hetzer, J., Forrest, M., Ribalaygua, J., Prado-López, C. & Hickler, T. The fire weather in Europe: large-scale trends towards higher danger. *Environ. Res. Lett.* **19**, 084017 (2024).
57. Dupuy, J. et al. Climate change impact on future wildfire danger and activity in Southern Europe: a review. *Ann. For. Sci.* **77**, 1–24 (2020).
58. Brown, E. K., Wang, J. & Feng, Y. US wildfire potential: a historical view and future projection using high-resolution climate data. *Environ. Res. Lett.* **16**, 034060 (2021).

59. Liu, Y., Stanturf, J. & Goodrick, S. Trends in global wildfire potential in a changing climate. *For. Ecol. Manag.* **259**, 685–697 (2010).
60. Liu, Y., Goodrick, S. L. & Stanturf, J. A. Future U.S. wildfire potential trends projected using a dynamically downscaled climate change scenario. *For. Ecol. Manag.* **294**, 120–135 (2013).
61. Dowdy, A. J. et al. Future changes in extreme weather and pyroconvection risk factors for Australian wildfires. *Sci. Rep.* **9**, 10073 (2019).
62. Peng, X. et al. Projections of wildfire risk and activities under 1.5 °C and 2.0 °C global warming scenarios. *Environ. Res. Commun.* **5**, 031002 (2023).
63. de Jong, M. C. et al. Calibration and evaluation of the Canadian Forest Fire Weather Index (FWI) System for improved wildland fire danger rating in the United Kingdom. *Nat. Hazards Earth Syst. Sci.* **16**, 1217–1237 (2016).
64. Rodriguez, H. et al. Towards the operational implementation of the Fire Weather Index FWI based on the High-Resolution WRF Model. in *2018 IEEE Biennial Congress of Argentina (ARGENCON)* 1–6. https://doi.org/10.1109/ARGENCON.2018.8645974 (2018).
65. Varela, V., Sfetsos, A., Vlachogiannis, D. & Gounaris, N. Fire Weather Index (FWI) classification for fire danger assessment applied in Greece. *Tethys* https://doi.org/10.3369/tethys.2018.15.03 (2015).
66. Keetch, J. J. & Byram, G. M. *A Drought Index for Forest Fire Control.* Res. Pap. SE-38, 35 p. 038 (U.S. Department of Agriculture, Forest Service, Southeastern Forest Experiment Station, 1968).
67. Noble, I. R., Gill, A. M. & Bary, G.aV. McArthur's fire-danger meters expressed as equations. *Aust. J. Ecol.* **5**, 201–203 (1980).
68. McArthur, A. G. Fire behaviour in Eucalypt forests. Conference paper Bulletin, (No. 107), Leaflet. Forestry Timber Bureau Australia, (35) (1967).
69. Pereira, M. G., Trigo, R. M., Da Camara, C. C., Pereira, J. M. C. & Leite, S. M. Synoptic patterns associated with large summer forest fires in Portugal. *Agric. For. Meteorol.* **129**, 11–25 (2005).
70. Météo France. *Bilan Climatique de l'été 2022*. https://meteofrance.fr/sites/meteofrance.fr/files/files/editorial/Bilan_complet_ete_2022_12102022.pdf (2022).
71. Jensen, D. et al. The sensitivity of US wildfire occurrence to pre-season soil moisture conditions across ecosystems. *Environ. Res. Lett.* **13**, 014021 (2018).
72. Mueller, S. E. et al. Climate relationships with increasing wildfire in the southwestern US from 1984 to 2015. *For. Ecol. Manag.* **460**, 117861 (2020).
73. O, S., Hou, X. & Orth, R. Observational evidence of wildfire-promoting soil moisture anomalies. *Sci. Rep.* **10**, 11008 (2020).
74. Westerling, A. L., Hidalgo, H. G., Cayan, D. R. & Swetnam, T. W. Warming and earlier spring increase Western U.S. Forest Wildfire Activity. *Science* **313**, 940–943 (2006).
75. Williams, A. P. et al. Correlations between components of the water balance and burned area reveal new insights for predicting forest fire area in the southwest United States. *Int. J. Wildland Fire* **24**, 14 (2015).
76. Rasilla, D. F., García-Codron, J. C., Carracedo, V. & Diego, C. Circulation patterns, wildfire risk and wildfire occurrence at continental Spain. *Phys. Chem. Earth Parts A/B/C.* **35**, 553–560 (2010).
77. Wang, X. et al. Critical fire weather conditions during active fire spread days in Canada. *Sci. Total Environ.* **869**, 161831 (2023).
78. Duane, A., Castellnou, M. & Brotons, L. Towards a comprehensive look at global drivers of novel extreme wildfire events. *Clim. Change* **165**, 43 (2021).
79. Seager, R. et al. Climatology, variability, and trends in the U.S. vapor pressure deficit, an important fire-related meteorological quantity. *J. Appl. Meteorol. Climatol.* **54**, 1121–1141 (2015).
80. Jain, P., Castellanos-Acuna, D., Coogan, S. C. P., Abatzoglou, J. T. & Flannigan, M. D. Observed increases in extreme fire weather driven by atmospheric humidity and temperature. *Nat. Clim. Chang.* **12**, 63–70 (2022).
81. Gutiérrez Rodríguez, L., He, Y., Sun, M., Yao, Y. & de Dios, V. R. Summer compound drought-heat extremes amplify fire-weather risk and burned area beyond historical thresholds in Chongqing Region, Subtropical China. *Fire* **6**, 346 (2023).
82. Turco, M., Llasat, M. C., von Hardenberg, J. & Provenzale, A. Impact of climate variability on summer fires in a Mediterranean environment (northeastern Iberian Peninsula). *Clim. Change* **116**, 665–678 (2013).
83. Flannigan, M. D. & Harrington, J. B. A study of the relation of meteorological variables to monthly provincial area burned by wildfire in Canada (1953–80). *J. Appl. Meteorol. Climatol.* **27**, 441–452 (1988).
84. Ministère de l'Agriculture et de la Souveraineté Alimentaire. BDIFF. *Base de Données sur les Incendies de Forêts en France (BDIFF)* https://bdiff.agriculture.gouv.fr/ (2024).
85. Abrhám, J., Soukupova, J. & Prochazka, P. Wildfires and tourism in the Mediterranean: balancing conservation and economic interests. *BioResources* **20**, 500–526 (2025).
86. Lanet, M., Li, L. & Le Treut, H. A framework to assess climate change effects on surface air temperature and soil moisture and application to Southwestern France. *Clim. Change* **177**, 170 (2024).
87. Zscheischler, J. et al. Future climate risk from compound events. *Nat. Clim. Change* **8**, 469–477 (2018).
88. IPCC. *Climate Change 2021: The Physical Science Basis. Contribution of Working Group I to the Sixth Assessment Report of the Intergovernmental Panel on Climate Change.* (Cambridge University Press, Cambridge, United Kingdom and New York, NY, USA, 2021). (in press).
89. Shepherd, T. G. et al. Storylines: an alternative approach to representing uncertainty in physical aspects of climate change. *Clim. Change* **151**, 555–571 (2018).
90. Landerer, F. W., Jungclaus, J. H. & Marotzke, J. Regional dynamic and steric sea level change in response to the IPCC-A1B scenario. *J. Phys. Oceanogr.* **37**, 296–312 (2007).
91. Fargeon, H. et al. Projections of fire danger under climate change over France: where do the greatest uncertainties lie?. *Clim. Change* **160**, 479–493 (2020).
92. Dosio, A., Spinoni, J. & Migliavacca, M. Record-breaking and unprecedented compound hot and dry summers in Europe under different emission scenarios. *Environ. Res. Clim.* **2**, 045009 (2023).
93. Felsche, E., Böhnisch, A., Poschlod, B. & Ludwig, R. European hot and dry summers are projected to become more frequent and expand northwards. *Commun. Earth Environ.* **5**, 1–11 (2024).
94. Ukkola, A. M., De Kauwe, M. G., Roderick, M. L., Abramowitz, G. & Pitman, A. J. Robust future changes in meteorological drought in CMIP6 projections despite uncertainty in precipitation. *Geophys. Res. Lett.* **47**, e2020GL087820 (2020).
95. Zhao, T. & Dai, A. CMIP6 model-projected hydroclimatic and drought changes and their causes in the twenty-first century. *J. Clim.* **35**, 897–921 (2022).
96. García-Valdecasas Ojeda, M. et al. Projected changes in the Iberian Peninsula drought characteristics. *Sci. Total Environ.* **757**, 143702 (2021).
97. Pausas, J. G. & Fernández-Muñoz, S. Fire regime changes in the Western Mediterranean Basin: from fuel-limited to drought-driven fire regime. *Clim. Change* **110**, 215–226 (2012).
98. Ma, W., Wilson, C. S., Sharples, J. J. & Jovanoski, Z. Investigating the effect of fuel moisture and atmospheric instability on PyroCb occurrence over Southeast Australia. *Atmosphere* **14**, 1087 (2023).
99. Richardson, D. et al. Increased extreme fire weather occurrence in southeast Australia and related atmospheric drivers. *Weather Clim. Extremes* **34**, 100397 (2021).
100. Tatli, H. & Türkeş, M. Climatological evaluation of Haines forest fire weather index over the Mediterranean Basin. *Meteorol. Appl.* **21**, 545–552 (2014).
101. Di Virgilio, G. et al. Climate change increases the potential for extreme wildfires. *Geophys. Res. Lett.* **46**, 8517–8526 (2019).

102. Tang, Y. et al. The potential impact of regional climate change on fire weather in the United States. *Ann. Assoc. Am. Geogr.* **105**, 1–21 (2015).
103. Varela, V. et al. Projection of forest fire danger due to climate change in the French Mediterranean region. *Sustainability* **11**, 4284 (2019).
104. Pimont, F. et al. Future expansion, seasonal lengthening and intensification of fire activity under climate change in southeastern France. *Int. J. Wildland Fire* **32**, 4–14 (2022).
105. Observatoire des territoires. Taux d'évolution annuel de la population. Observatoire des territoires https://www.observatoire-des-territoires.gouv.fr/outils/cartographie-interactive/#bbox=-239058,5750774,427165,227278&c=indicator&i=insee_rp_evol_1968.tx_var_pop&s=2014-2020&view=map59 (2024).
106. Carvalho, A. et al. The impact of spatial resolution on area burned and fire occurrence projections in Portugal under climate change. *Clim. Change* **98**, 177–197 (2010).
107. Davis, K. T. et al. Tamm review: A meta-analysis of thinning, prescribed fire, and wildfire effects on subsequent wildfire severity in conifer dominated forests of the Western US. *For. Ecol. Manag.* **561**, 121885 (2024).
108. Guo, Y., Wang, J., Ge, Y. & Zhou, C. Global expansion of wildland-urban interface intensifies human exposure to wildfire risk in the 21st century. *Sci. Adv.* **10**, eado9587 (2024).
109. Spyratos, V., Bourgeron, P. S. & Ghil, M. Development at the wildland–urban interface and the mitigation of forest-fire risk. *Proc. Natl. Acad. Sci. USA* **104**, 14272–14276 (2007).
110. Schug, F. et al. The global wildland–urban interface. *Nature* **621**, 94–99 (2023).
111. Radeloff, V. C. et al. Rapid growth of the US wildland-urban interface raises wildfire risk. *Proc. Natl. Acad. Sci. USA* **115**, 3314–3319 (2018).
112. Hertelendy, A. J. et al. Seasons of smoke and fire: preparing health systems for improved performance before, during, and after wildfires. *Lancet Planet. Health* **8**, e588–e602 (2024).
113. Synolakis, C. E. & Karagiannis, G. M. Wildfire risk management in the era of climate change. *PNAS Nexus* **3**, pgae151 (2024).
114. Boomhower, J. Adapting to growing wildfire property risk. *Science* **382**, 638–641 (2023).
115. McWethy, D. B. et al. Rethinking resilience to wildfire. *Nat. Sustain* **2**, 797–804 (2019).
116. Tedim, F., Leone, V. & McGee, T. K. *Extreme Wildfire Events and Disasters: Root Causes and New Management Strategies* (Elsevier, 2019).
117. Chevallier, P. et al. Current and future water balance of a mountain subcatchment of Issyk-Kul Lake, Tien Shan range, Kyrgyzstan. *Sci. Total Environ.* **897**, 165363 (2023).
118. Hausfather, Z. & Peters, G. P. Emissions—the 'business as usual' story is misleading. *Nature* **577**, 618–620 (2020).
119. Ma, F. & Yuan, X. Impact of climate and population changes on the increasing exposure to summertime compound hot extremes. *Sci. Total Environ.* **772**, 145004 (2021).
120. Jacob, D. et al. EURO-CORDEX: new high-resolution climate change projections for European impact research. *Reg. Environ. Change* **14**, 563–578 (2014).
121. Strandberg, G. et al. *CORDEX Scenarios for Europe from the Rossby Centre Regional Climate Model RCA4*. SMHI Report Meteorology and Climatology 116 (2014).
122. Hazeleger, W. et al. EC-Earth: a seamless Earth-system prediction approach in action. *Bull. Am. Meteorol. Soc.* **91**, 1357–1364 (2010).
123. Giorgetta, M. A. et al. Climate and carbon cycle changes from 1850 to 2100 in MPI-ESM simulations for the Coupled Model Intercomparison Project phase 5. *J. Adv. Model. Earth Syst.* **5**, 572–597 (2013).
124. The HadGEM2 Development Team, Martin, G. M. et al. The HadGEM2 family of Met Office Unified Model climate configurations. *Geosci. Model Dev.* **4**, 723–757 (2011).
125. Benestad, R. E. & Haugen, J. E. On complex extremes: flood hazards and combined high spring-time precipitation and temperature in Norway. *Clim. Change* **85**, 381–406 (2007).
126. Hao, Z. & AghaKouchak, A. A nonparametric multivariate multi-index drought monitoring framework. *J. Hydrometeorol.* **15**, 89–101 (2014).
127. Yue, S. & Rasmussen, P. Bivariate frequency analysis: discussion of some useful concepts in hydrological application. *Hydrol. Process.* **16**, 2881–2898 (2002).
128. Vrac, M., Thao, S. & Yiou, P. Changes in temperature–precipitation correlations over Europe: are climate models reliable?. *Clim. Dyn.* **60**, 2713–2733 (2023).

Acknowledgements

The authors are grateful to the World Climate Research Program's Working Group on Coupled Modelling, which is responsible for CMIP6, and to the modelling communities for producing and making available their model outputs. All the simulations are publicly available on a website (https://esgf-node.llnl.gov/projects/cmip6/). They are also grateful to the Copernicus Climate Change Service for making publicly available the datasets used in this article. To process the CMIP6 data, this study benefited from GENCI computing resources and from the IPSL mesocenter ESPRI facility which is supported by CNRS, UPMC, Labex L-IPSL, CNES and Ecole Polytechnique. The authors acknowledge support from the European NBRACER project (Horizon Programme under grant agreement 101112836).

Author contributions

M.L. conceived the study and analysed the data. L.L. and H.L. provided feedback and comments on the initial paper written by M.L. All authors contributed to interpreting the results and improving the paper.

Competing interests

The authors declare no competing interests.

Additional information

Supplementary information The online version contains supplementary material available at https://doi.org/10.1038/s44304-025-00124-0.

Correspondence and requests for materials should be addressed to Marine Lanet.